Cylindrical samples of brick masonry with aerial lime mortar under compression: experimental and numerical study

Luca Pelà*, Savvas Saloustros, Pere Roca

Department of Civil and Environmental Engineering, Universitat Politècnica de Catalunya (UPC-BarcelonaTech), Jordi Girona 1-3, 08034 Barcelona, Spain

* Corresponding author. Phone: +34 934011036

Fax: +34 934054135

luca.pela@upc.edu

Abstract – This research presents an experimental and numerical study focusing on the compression test of cylindrical samples core drilled from existing masonry walls. This method is suitable for the minor destructive assessment of the mechanical properties of historical masonry, like that composed of aerial lime mortar joints and solid clay bricks. This particular material combination, frequently found in the vast majority of the built cultural heritage, was utilized to build representative specimens that were stored in the laboratory for one year until their testing. Cylindrical samples of 150 mm diameter were extracted from the masonry walls by using a dry core-drilling procedure, and then regularized to be tested under compression in the laboratory. A comparison is presented between the experimental results on cylindrical samples and those obtained from standard compression tests on prismatic samples consisting in stack bond prisms. Numerical simulations by finite element micro-modelling of the compression tests on the core samples were carried out to investigate the experimental behaviour of the specimens and evaluate the compressive strength of the material from this nonstandard technique. The combined experimental and numerical study allows the assessment of important mechanical parameters for the compressive characterisation of masonry composed of aerial lime mortar joints and solid clay bricks.

Keywords: Brickwork; Coring; In-situ; Sampling; Minor Destructive Testing (MDT); Compressive Strength; Finite Element Method; Micro-modelling; Continuum Damage Mechanics; Damage.

Abbreviations - MDT: Minor Destructive Testing; 2JC: Two-Joint Cylinder; 3JC: Three-Joint Cylinder; LVDT: Linear Variable Differential Transformer, DPT: Double Punch Test.

1. Introduction

The knowledge of the compressive behaviour of masonry is essential in the current design practice [1]. However, the assessment of the compressive mechanical properties of masonry can be rather challenging in studies involving the assessment of existing

34 historical buildings due to the need to minimize possible damage induced to the structure

35 by the inspection procedures.

36 For this type of constructions, a rather recurrent material is the combination of lime mortar

37 joints and solid clay bricks. Experimental studies about this type of masonry are of

38 paramount importance for people involved in the analysis and restoration of historical

39 structures. However, the possibility of laboratory tests on newly manufactured lime

40 mortar samples encounters a significant difficulty in the long curing and hardening

41 periods [2–4]. In spite of this difficulty, some methods have been proposed to characterise

42 masonry as a composite material based on the mechanical properties of the material

43 components, i.e. lime mortar and brick units. The analysed masonry samples are usually

44 prismatic as those required by current technical standards [5,6], e.g. stack bond prisms

45 [7,8], small columns [9,10] and Flemish bond wallets [8,11–13].

46 More recent works focus on laboratory testing of cylindrical samples core-drilled from

47 lime mortar and clay brick masonry walls [14–17]. This minor destructive testing (MDT)

48 method was suggested by the UIC 778-3 recommendations [18] and has shown to be

49 suitable for the assessment of the mechanical properties of existing structures due to its

50 limited invasiveness [19–21]. The extraction of cylindrical samples from existing

51 masonry walls is more appropriate than cutting prismatic wallets, as those recommended

52 by standards for new construction [5,6]. The main reason is that core drilling provides

53 undamaged cylindrical masonry samples, easy to transport and maintain intact until the

54 delivery to the laboratory. This favourable feature can ensure a reliable evaluation of

55 compressive strength from undisturbed specimens. On the contrary, the prismatic wallets

56 cut from existing brickwork are normally prone to damage during the extraction

57 operations, consisting typically in the combined use of a circular saw and a chisel, as well

58 as during the transport to the laboratory.

59 There is, however, the need for experimental criteria to correlate the results obtained from

60 this novel non-standard method with those referring to the standard compression tests on

61 prismatic samples. For this reason, reference laboratory tests on walls replicating

62 historical-like materials seem necessary to gain further knowledge about the correct

63 execution of core sampling, experimental setup and testing, results processing and

64 derivation of mechanical parameters for the compressive characterisation. In particular,

65 benchmark studies are needed about the application of this MDT technique to aerial lime

66 mortar and solid brick masonry, a traditional material of the built heritage. The available

67 numerical methods, such as those based on finite element micro-modelling [22,23], may

68 also help to interpret the mechanical behaviour of masonry cylindrical specimens by
69 advanced computational simulations of their resisting mechanism under compressive
70 loading.

71 The main objective of this research is to provide comprehensive experimental results
72 supported by numerical simulations about the compressive behaviour of cylindrical
73 specimens of aerial lime mortar and terracotta brick masonry. Compression tests were
74 carried out by considering cylindrical samples core-drilled from walls replicated in the
75 laboratory, together with standard stack bond prisms. The extraction of cylindrical
76 specimens was executed one year after the construction of the walls, by using a dry core
77 drilling technique to avoid disjointing between low strength mortar joints and units. The
78 regularization of cylindrical samples was carried out by means of high-strength mortar
79 caps [14,15] in order to allow the application of the compressive load over the
80 investigated material. Two different cylindrical specimens were tested, including either
81 four brick pieces (with two horizontal mortar joints and a vertical one) or three brick
82 pieces (with two horizontal mortar joints). The results from compression tests on core
83 samples and prismatic specimens are finally compared in an attempt to provide
84 experimental correlations among the different types of specimens.

85 The experimental calibration of this MDT technique is pursued in order to provide reliable
86 procedures for its possible application to existing structures of the built heritage. The
87 presentation of advanced numerical simulations by finite element micro-modelling aims
88 to give insights into the experimental behaviour of the extracted cylindrical specimens
89 when tested under compression, regarding their resisting mechanism and type of failure.

90 ## 2. Experimental program

91 The experimental program was executed at the Technical University of Catalonia (UPC-
92 BarcelonaTech) in the Laboratory of Technology of Structures and Building Materials.
93 This section presents in detail the characterisation of the material components, the
94 masonry specimens and the testing setups.

95 ### 2.1 Characterisation of construction materials

96 One of the most important aspects of the experimental campaign was the choice of the
97 material components for building the specimens. In order to reproduce historical
98 materials, pure aerial lime mortar CL90 without cement [24] and handmade terracotta

bricks were used (Figure 1). The mortar was prepared by using a volume ratio of binder to aggregate of 1:3 (lime:sand), while the content of water was defined by the workmanship in order to achieve an optimum workability of the mixture. The adopted silica sand had a grain size distribution of $0 \div 2$ mm.

The mortar's flexural (f_{fm}) and compressive (f_{cm}) strengths were measured on prisms with dimensions $160 \times 40 \times 40$ mm^3 (Figure 1a) according to [25]. Four specimens were provided for the flexure test. Eight halves, resulting from the prisms splitted after the four flexure tests, were tested under compression with 40×40 mm^2 steel loading platens (Figure 1c). The tests were performed with a 10 kN load cell under load control. The rate of the applied load was constant during each test with values of 10 N/s for the flexure tests and 50 N/s for the compression tests. Table 1 presents the results obtained one year after the pouring of mortar. The average value of flexural strength was $f_{fm} = 0.55$ MPa and that of compressive strength was $f_{cm} = 1.63$ MPa, with coefficients of variation (CV) of 9.5% and 5.3% respectively. These results seem reasonable if compared with the strength values from previous studies on lime mortar available in the literature [2,3].

Figure 1 – Flexure and compression testing of prismatic samples of mortar (a,c) and brick (b,d). Double punch testing of mortar joints (e).

120 Table 1 – Experimental flexural and compressive strengths derived from prisms of aerial lime mortar.

Mortar CL90 sample	f_{fm} (MPa)	f_{cm} (MPa)
1	0.48	1.70
		1.54
2	0.52	1.47
		1.72
3	0.60	1.63
		1.72
4	0.60	1.68
		1.58
Average	0.55	1.63
CV %	9.5	5.3

121

122 Masonry specimens were built using handmade terracotta bricks with nominal
123 dimensions $305 \times 145 \times 45$ mm^3. Six units were tested under compression according to
124 [26], with a machine equipped with a 3000 kN load cell. The average value of the
125 compressive strength of units was $f_{cb,u} = 30.7$ MPa with CV=5.6%. The normalized
126 uniaxial compressive strength of the bricks resulted 21.49 MPa, after applying the shape
127 factor equal to 0.7 as recommended by the standard [26]. Six cubes cut from the units
128 were also tested in compression (Figure 1d), providing an average value of the
129 compressive strength of $f_{cb,c} = 18.4$ MPa, with CV=5.9%. The difference between the
130 average compressive strengths measured in the entire units and in the smaller cubes is
131 due to the very different aspect ratios of the two specimens [27], as the entire brick is
132 subjected to much higher transversal confinement exerted by the loading plates of the
133 testing machine than the cube sample. Sixteen brick prisms were tested under flexure to
134 evaluate the flexural strengths along the header and stretcher directions (Figure 1b),
135 providing average values $f_{fb,x} = 3.63$ MPa (CV=3.7%) and $f_{fb,y} = 3.79$ MPa (CV=13.1%),
136 respectively. The reference standard considered was the same adopted for mortar prisms
137 [25] due to the lack of specific guidelines for flexure test of brick samples. The
138 experimental results for brick samples are summarised in Table 2. These results seem
139 reasonable if compared with the strength values from previous studies on solid clay bricks
140 available in the literature [11–13].

141

142

143

144

145

146

Table 2 – Experimental compressive and flexural strengths of bricks

Brick Sample	$f_{cb,u}$ (MPa)	$f_{cb,c}$ (MPa)	$f_{fb,x}$ (MPa)	$f_{fb,y}$ (MPa)
1	31.2	19.6	3.81	3.81
2	29.4	19.5	3.67	3.53
3	30.4	19.1	3.60	3.57
4	30.3	18.3	3.52	3.74
5	34.2	16.6	3.51	3.19
6	28.9	17.5	3.59	3.32
7			3.88	4.40
8			3.48	4.73
Average	30.7	18.4	3.63	3.79
CV %	5.6	5.9	3.7	13.1

147

148 The mechanical parameters derived from standard tests show that the present
149 experimental campaign adopted component materials with low-to-moderate properties,
150 especially for the lime mortar [2,3]. The handmade terracotta units, due to their traditional
151 manufacturing process, provided strength values much lower than the modern bricks
152 produced for the construction of new masonry [23].

153 **2.2 Construction of masonry specimens**

154 Two walls with dimensions $1605 \times 870 \times 145$ mm^3 were built in stretcher bond (Figure
155 2a) using the materials detailed in Section 2.1. The construction was intended to
156 reproduce a wall with low strength mortar, typical of historical masonry buildings. The
157 two walls were constructed in the present research to allow the simulation of in-situ core-
158 drilling of 150 mm diameter cylindrical specimens. The walls were built over a steel
159 beam. At the end of their construction, a regularization layer of mortar was poured over
160 the wall, to permit the location of another steel beam. The top and the bottom steel profiles
161 were then connected by two low-tensioned bars in both faces of the walls. The sole
162 purpose of this pre-compression was to provide sufficient confinement to the walls in
163 order to avoid their damage during the laboratory operations, like transportation of
164 samples and coring.
165 Six stack bond prisms were built with the same materials during the construction of the
166 walls. The stack bond prisms consisted of five bricks and four mortar bed joints with
167 dimensions $305 \times 305 \times 145$ mm^3 (Figure 2b). The top and the bottom surfaces of the
168 prisms were coated with a thin regularization layer of high-strength cement mortar, to
169 ensure the uniform distribution of the compressive load as established by [5].

170
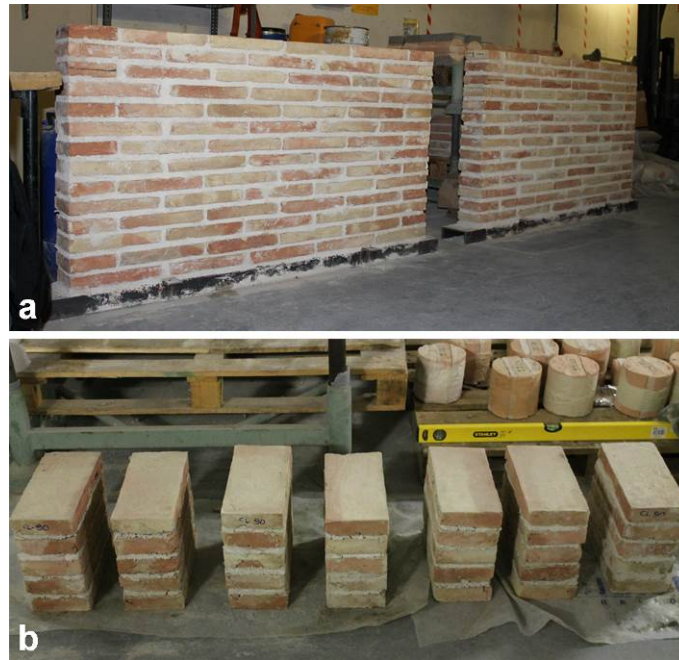
171

172 Figure 2 – Construction of specimens in the laboratory: (a) masonry walls and (b) stack bond prisms.

173

174 The operations of extraction of cylindrical samples started after one year of curing, after

175 taking out the walls of their storage. At that moment, the aerial lime mortar showed to

176 have reached a proper level of carbonation, as proved by the use of phenolphthalein

177 indicator solution, as well as a sufficient strength, as derived from the prismatic

178 specimens, see Table 1. The core-drilling was executed using a dry procedure, i.e. without

179 water (Figure 3a). This solution showed several advantages in recent research by the

180 authors [16] compared with the traditional wet procedures that spoil the samples by

181 washing the mortar joints away. The drilling machine induced only a rotation to the

182 diamond bit, avoiding any excess of vibration that may cause the formation of internal

183 cracks within the cylindrical specimen. The position of the extracted cylinders was

184 decided in order to provide as many specimens as possible. Coring operations were

185 carefully executed in order to avoid undesirable disjointing of specimens. The procedure

186 was subdivided into different stages. First, the machine drilled until the half of the

187 thickness of the wall. Second, the dust produced by the drilling was removed from the

188 interior of the core bit and from the prints on the wall. The drilling operation was

189 eventually completed through the whole thickness of the wall. The cylinders were

190 carefully extracted from the core bit and immediately confined with strong adhesive tape

191 stuck on their lateral curved surface. They were finally stored in the laboratory to be

192 tested. Figure 3b shows the remaining wall after the core-drilling. It is worth noticing the

193 absolute absence of water as well as the reduced amount of dust due to the use of the
194 vacuum cleaner connected to the drilling equipment. Therefore, the operations of
195 extraction of samples proved to be usefully clean.
196
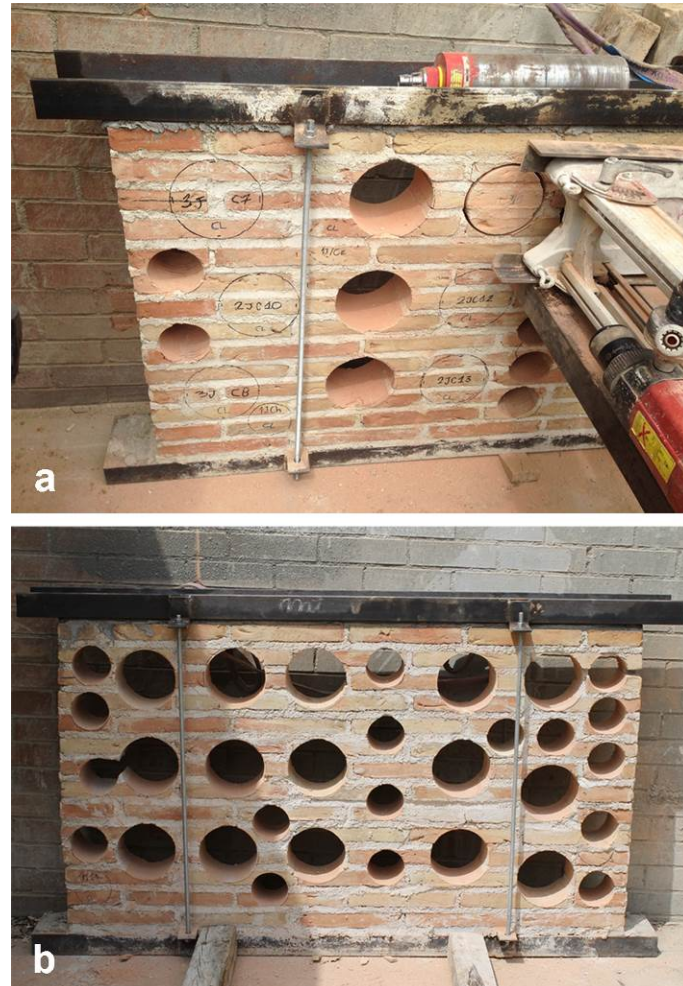
198 Figure 3 – Extraction of the cylindrical specimens of masonry: (a) core drilling and (b) wall after the
199 extraction.
200

201 Three types of specimens were extracted from the walls. First, 150 mm diameter cores
202 with three brick pieces and two horizontal mortar joints, called 2JCs (two-joint cylinders)
203 (Figure 4a). Second, 150 mm diameter cores including four brick pieces, two horizontal
204 mortar joints, and a vertical mortar joint, called 3JCs (three-joint cylinders) (Figure 4b).
205 Finally, 90 mm diameter cores with a mortar diametric joint between two brick cylindrical
206 segments that were employed in another experimental study [17]. The 2JCs and the 3JCs
207 were used for the compression test following the procedures presented in [14,15]. Even

though fifteen 2JCs and fifteen 3JCs were extracted successfully, compression tests were executed on six 2JCs and six 3JCs.

The 2JCs and 3JCs were regularized with mortar caps of 105 mm width made of high strength mortar, shaped by means of special wooden moulds (Figure 4c). The average value of compressive strength for the regularization mortar after 28 days was 65 MPa and thus much higher than the one expected from masonry core samples. The curved lateral surface of the cylinders was regularized to create two plane surfaces parallel to the bed joints to be loaded by vertical compression. The specimens were stored in the laboratory conditions and, once hardened, extracted from the moulds to be tested (Figure 4d). This regularization ensures an optimal transmission of the compressive force from the testing machine to the specimen through a perfectly adherent high-strength cap, therefore avoiding possible stress concentrations [14]. This specific approach is different from the one proposed by UIC guidelines [18] and other relevant works [20] which used metal concave pieces gripped to the testing machine.
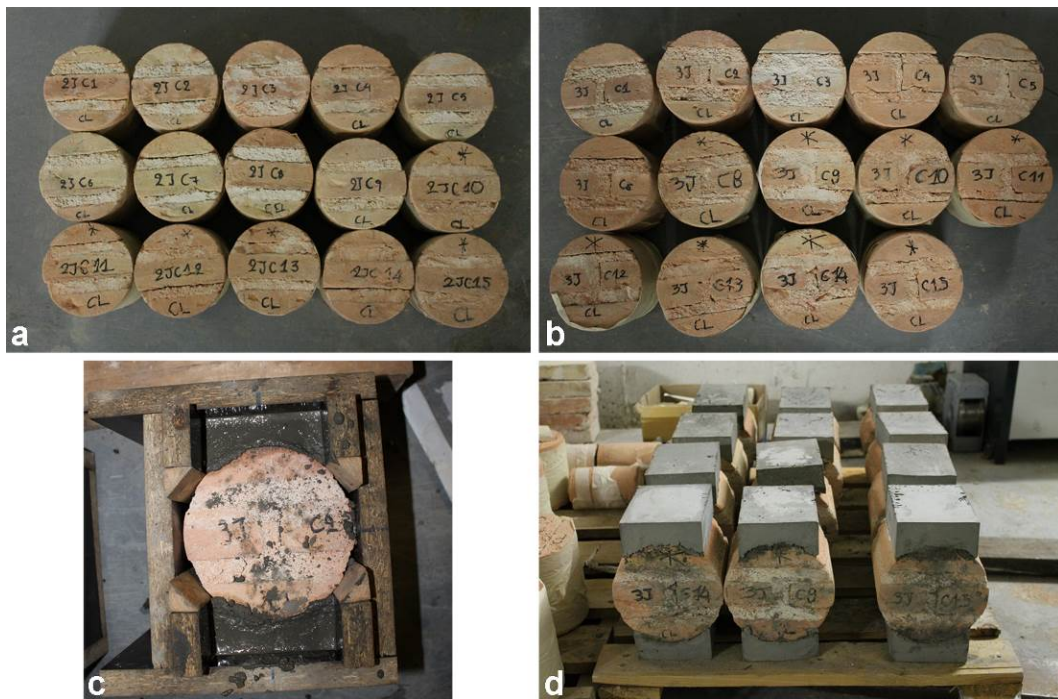
Figure 4 – Cylindrical specimens obtained from core-drilling of the wall: (a) two-joint cylinders, (b) three-joint cylinders, (c) regularization by mortar capping, (d) samples ready for testing.

2.3 Characterisation of mortar joints

Additionally to the compression tests on mortar prisms detailed in Section 2.2, the compressive strength of the aerial lime mortar in the joints of the walls was evaluated

229 through the double punch test (DPT) following the DIN 18555-9:1999 standards [28] as
230 well as references [18,29]. After the execution of core drilling, the remaining walls with
231 holes in them (Figure 3b) were dismantled very cautiously course by course by using a
232 very small chisel, in order to extract carefully the mortar slabs. Mortar samples with
233 dimensions roughly $50 \times 50 \times 18$ mm^3 were extracted from the joints of the masonry
234 walls after the extraction of the core samples. Gypsum powder was used to regularize the
235 irregular faces of the mortar samples, placed between loading platens with 20 mm
236 diameter (Figure 1e). The loading rate of the testing machine was 0.0094 kN/s and the
237 load cell had a capacity of 10 kN.
238 Table 3 presents the results of the 11 tested mortar joint samples. The average
239 compressive strength measured with the DPT was $f_{cm,DPT} = 0.91$ MPa, with CV=24%.
240 This value is lower than the average compressive strength derived from the standard
241 prismatic specimens (1.63 MPa, see Table 1), even though the joint samples had lower
242 thickness. This difference is due to the diverse curing conditions of the two typologies of
243 mortar specimens. The aerial lime hardens when exposed to air and the mortar joints of
244 the wall had a much lower external exposed surface, with a limited thickness of around
245 18 mm, than the $160 \times 40 \times 40$ mm^3 prismatic mortar samples conforming with the
246 standards [25]. For this reason, the development of the strength in the mortar joints was
247 slower than in the standard prisms. In addition, the joints were built in contact with the
248 bricks' surfaces, whereas the prismatic samples were casted into steel moulds. The initial
249 moisture of the bricks during the construction of the walls might also influence the
250 evolution of the strength of the joints. All the mentioned factors may also explain the
251 higher CV in DPT tests than in the standard compressive ones, together with the
252 unavoidable geometric irregularity of the joint samples extracted from the walls.
253 The previous observations suggest that the DPT provided a more realistic evidence of the
254 actual compressive strength reached by the aerial lime mortar joints within the wall, since
255 the compressive strength derived from standard prismatic samples was affected by
256 different curing conditions and thus exhibited different physical and mechanical
257 properties.
258
259
260
261
262

263   Table 3 - Experimental strengths from double punch tests on mortar joints extracted from the walls.

Mortar CL90 joint sample	$f_{cm,DPT}$ (MPa)
1	0.87
2	1.48
3	0.80
4	0.93
5	1.28
6	0.92
7	1.07
8	0.88
9	0.99
10	0.67
11	1.02
Average	0.91
CV%	24.0

264   **2.4 Testing setups**

265   All the specimens, i.e. core samples and stack bond prisms, were tested under
266   compression one year after their construction [30].

267   The compression tests of six 2JCs and six 3JCs were executed according to the procedures
268   reported in [14,18]. The tests consisted in applying a compressive loading on the
269   regularization caps perpendicularly to the bed joints (Figure 5a). The compression
270   machine was equipped with a 200 kN load cell. Both the vertical and horizontal
271   displacements were recorded through four linear variable differential transformers
272   (LVDTs). Two vertical LVDTs (±5 mm range and 5 μm precision) were attached to the
273   regularization caps, two horizontal LVDTs (±1.5 mm range and 1.5 μm precision) were
274   placed horizontally in the front faces of the specimens and two horizontal LVDTs (±5
275   mm range and 5 μm precision) were fixed on two external metal supports along the
276   diametric direction of the specimen. The test was divided into two stages, corresponding
277   to elastic loading/unloading and then loading beyond the failure. The first stage was
278   performed under load control by carrying out three loading/unloading cycles in order to
279   evaluate the elastic response of masonry. The cycles were performed between the 5% and
280   20% (3 kN ÷ 20 kN) of the originally expected maximum load. The second loading stage
281   was performed under displacement control, at a rate of 0.004 mm/s. This last stage
282   allowed to measure the compressive strength of the sample and to characterise its
283   softening behaviour. The Young's modulus of masonry was evaluated from the last
284   loading/unloading cycle, using the measurements from the two vertical LVDTs placed on
285   the specimens.

286   The stack bond prisms were tested under compression loading in order to compare the
287   results with those from the core samples. The standard [6] was followed for the testing
288   procedures. The samples were regularized with a 10 mm layer of high strength mortar on
289   the upper and lower parts to ensure the uniform loading distribution during the test. The
290   compression machine was equipped with a 3000 kN load cell. Six LVDTs were used to
291   measure vertical and horizontal displacements, according to [5] (Figure 5b). Four vertical
292   LVDTs (±5 mm range and 5 μm precision) were stuck on each lateral face of the prism
293   and two horizontal LVDTs (±1.5 mm range and 1.5 μm precision) were stuck on the two
294   larger lateral faces of the prism. Three initial loading cycles under force control were
295   executed between the 5% and 33% (11 kN ÷ 73 kN) of the expected maximum load. The
296   latter was estimated by using the equation suggested by the Eurocode 6 [31] based on the
297   individual strengths of the masonry components. The second loading stage was performed
298   under displacement control, with a rate of 0.008 mm/s, in order to reach the compressive
299   strength and then to follow the post-peak response of masonry.
300
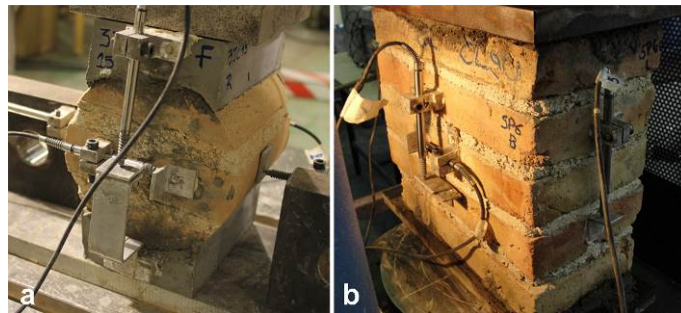
301

302   Figure 5 – Experimental setups for compression tests on: (a) core samples and (b) stack bond prisms.

3. Experimental results

304   This section summarizes the main results of the experimental campaign. Standard and
305   non-standard compression tests provided a meaningful set of data that can be analysed to
306   evaluate the mechanical parameters of the investigated materials. The outcomes of the
307   tests from all the specimens were used to evaluate the compressive strength and the elastic
308   parameters of the studied masonry.

3.1 Compression tests on core samples

310   The compressive stress acting on the cylindrical specimens was evaluated considering
311   two different values. The stress value σ_1 was calculated by considering the total diametric

312   section of the cylinder, while the stress value σ_2 was obtained by using the section of the
313   regularization cap. The first approach is the one suggested by the UIC 778-3
314   recommendations [18] to calculate the compressive strength of masonry from cylindrical
315   specimens. It considers the entire horizontal cross section of the specimen as the resistant
316   section until reaching the maximum load. The second approach has been investigated in
317   previous research by the authors [14,15] and it is also considered herein, in addition to
318   the first one, to evaluate the compressive strength. This second approach is suggested by
319   the experimental evidence of the crack pattern shown by the specimens close to failure.
320   According to this evidence, observed in all tests, the specimens experience cracking and
321   subsequent detachment of the lateral less confined portions of material. Close to failure,
322   the compressive stresses are concentrated in a sand cone shape limited by the cracks
323   developed. As a result, the effective resisting cross-section of the cylinder may be smaller
324   than the total horizontal one.
325   Figure 6 shows the stress-strain curves calculated for the first stage of loading/unloading
326   for both 2JCs and 3JCs, as well as the curves obtained for the last loading stage beyond
327   failure. As mentioned, the loading/unloading cycles were used to evaluate the Young's
328   modulus of the material. They were evaluated making reference to both σ_1 and σ_2 values,
329   leading to the definition of the relevant values E_1 and E_2.
330   As for the evaluation of the compressive strength values, the value f_{C1} was defined
331   considering the maximum force divided by the diametric cross-section of the cylinder,
332   while the value f_{C2} was obtained considering the maximum force divided by the cross-
333   section of the regularization cap. The relevant expressions are:

334   $$f_{C1} = \frac{F_{max}}{\phi l} \qquad f_{C2} = \frac{F_{max}}{bl} \qquad\qquad\qquad (1a,b)$$

335   in which b is the width of the mortar cap, l is the length of the cylinder and ϕ its diameter.
336
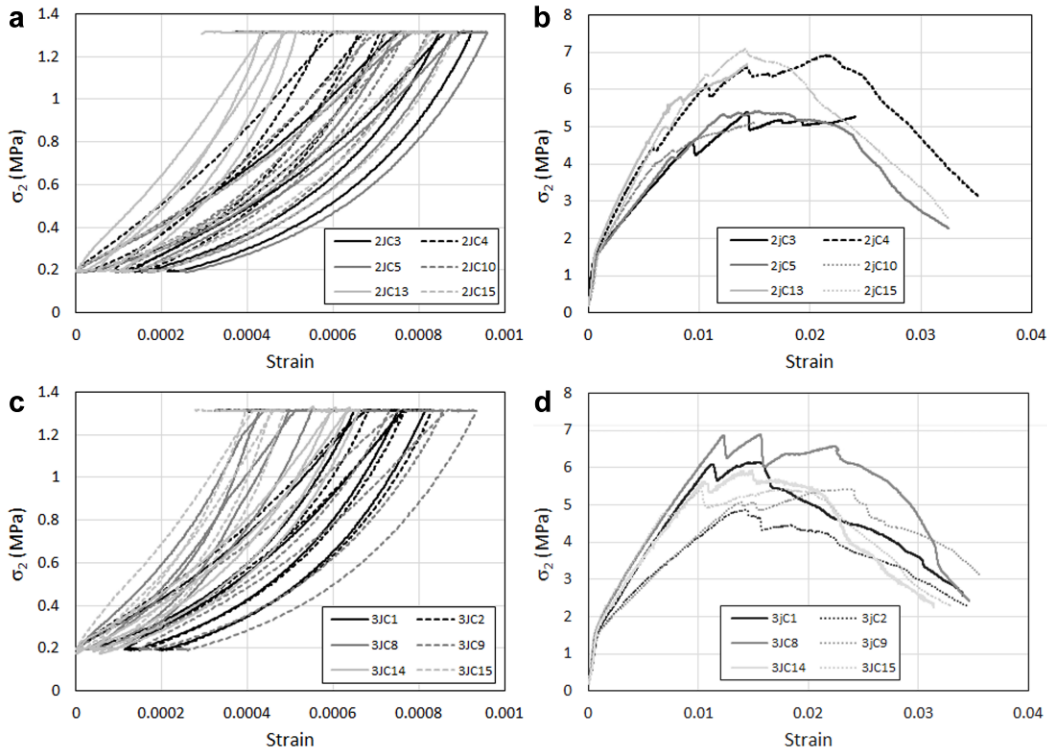
Figure 6 – Stress vs. strain curves of core samples: elastic loading/unloading cycles for two-joint (2JC) (a) and three-joint cylinders (3JC) (c); loading beyond failure for two-joint (b) and three-joint cylinders (d).

Table 4 presents a summary of the experimental results from compression tests on core samples. As for the values of f_{C1} and f_{C2}, the 2JCs provided average values of 4.25 MPa and 6.17 MPa, whereas the 3JCs provided average values of 3.98 MPa and 5.78 MPa, respectively. As for the values of E_1 and E_2, the 2JCs provided average values of 1182 MPa and 1716 MPa, whereas the 3JCs provided average values of 1323 MPa and 1921 MPa, respectively.

Table 4 – Experimental results of compression tests on core samples in terms of compressive strengths and Young's moduli.

| Sample 2JC	f_{C1} (MPa)	f_{C2} (MPa)	E_1 (MPa)	E_2 (MPa)	Sample 3JC	f_{C1} (MPa)	f_{C2} (MPa)	E_1 (MPa)	E_2 (MPa)
2JC3	3.72	5.40	1007	1463	3JC1	4.23	6.15	1137	1652
2JC4	4.76	6.91	1272	1848	3JC2	3.36	4.88	1127	1637
2JC5	3.73	5.42	985	1431	3JC8	4.74	6.89	1588	2306
2JC10	3.58	5.20	1109	1610	3JC9	3.73	5.42	1019	1479
2JC13	4.82	7.00	1707	2479	3JC14	4.08	5.92	1254	1822
2JC15	4.88	7.09	1009	1466	3JC15	3.74	5.43	1811	2631
Average	4.25	6.17	1182	1716	Average	3.98	5.78	1323	1921
CV %	13.6	13.6	21.5	21.5	CV %	11.04	11.05	21.4	21.4

350 Both the 2JCs and 3JCs presented a typical sandglass failure after the compression test
351 (Figure 7). All the specimens, after reaching the peak of the compressive load, exhibited
352 cracks in correspondence with the edges of the regularization cap, which created two
353 lateral wings falling off from the specimens. At the end of the test, the remaining central
354 part of the specimens was hourglass shaped, with upper and lower sections equal to those
355 of the regularization caps, and central one smaller than the extreme ones.
356
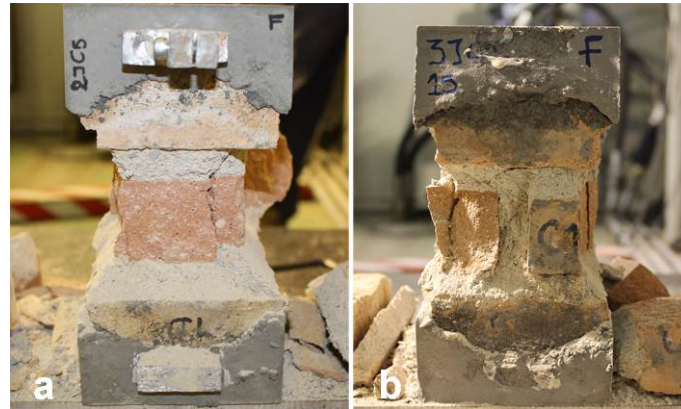
358 Figure 7 – Typical hourglass failure exhibited by core samples after the compression tests: (a) two-joint
359 and (b) three-joint cylinders.
360

3.2 Compression tests on stack bond prisms

362 Figure 8 shows the stress-strain curves calculated for the first stage of loading/unloading
363 for stack bond prisms, as well as the curves obtained for the following monotonic loading
364 stage until failure. The post peak branch was not measured in specimens SBP2, SBP4 and
365 SBP5, as the vertical LVDTs either detached at the maximum force or were removed to
366 avoid their damaging during the completion of the test in the softening stage.
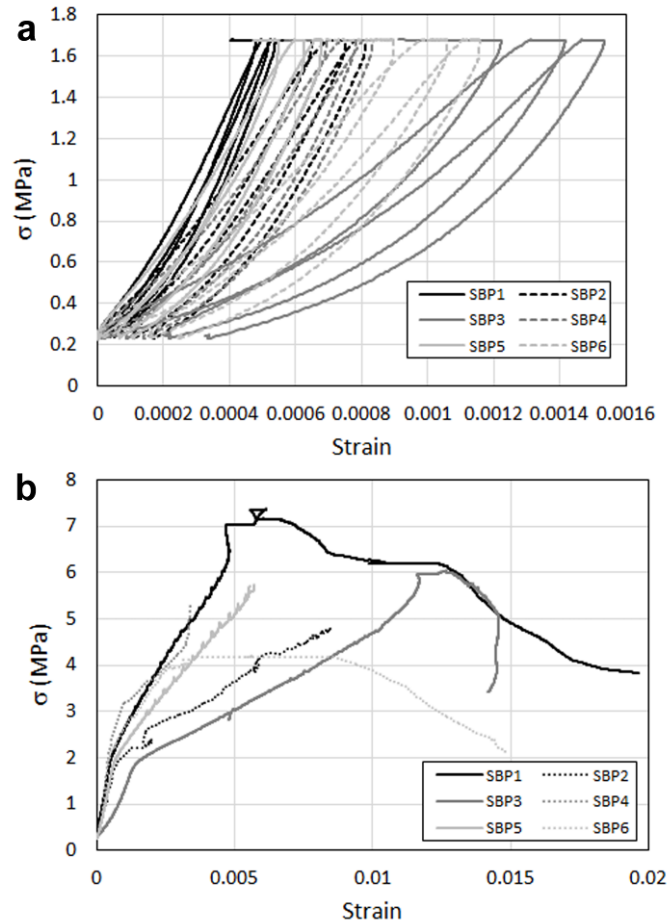
Figure 8 – Stress vs. strain curves of stack bond prisms: elastic loading/unloading cycles (a) and loading beyond failure (b).

Table 5 shows the summary of the compression tests on stack bond prisms in terms of compressive strength and elastic parameters. The average compressive strength of stack bond prisms was 5.79 MPa, whereas the Young's modulus was 2014 MPa. The evaluation of the elastic parameters was possible for all the specimens. All the six stack bond prisms showed a similar failure mode. First, cracks appeared in the central bricks and then propagated towards the upper part of the specimens. All the cracks were vertical and crossed almost all the height of the prism, as expected from a compression test. Extensive cracks appeared also in the lateral fragments. Several substantial cracks appeared on both sides of the prisms (Figure 9).
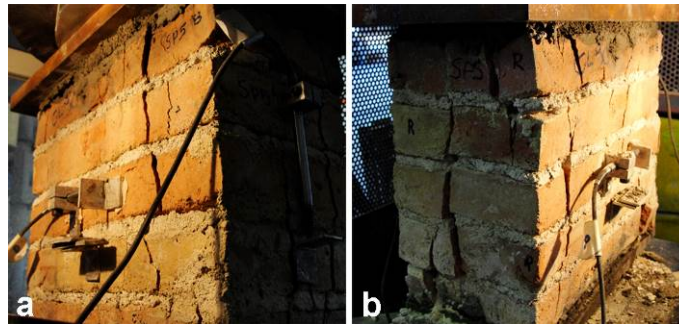
383   Table 5 – Experimental results of compression tests on stack bond prisms in terms of compressive
384   strengths and Young's moduli.

Stack Bond Prism	f_C (MPa)	E (MPa)
SBP1	7.37	2850
SBP2	4.98	2055
SBP3	6.05	1098
SBP4	5.97	1940
SBP5	6.15	2685
SBP6	4.20	1453
Average	5.79	2014
CV %	17.2	30.8

385

386

387   Figure 9 – Typical failure exhibited by stack bond prisms after the compression tests: (a) front, (b) back
388   and lateral sides.

3.3 Discussion

390 Figure 10 shows the comparison of the experimental results for prismatic and cylindrical

391 samples, in terms of average values of Young's modulus and compressive strength.

392 The values of the Young's modulus of the investigated lime mortar masonry ranged

393 between 1182 MPa and 2014 MPa, depending on the type of sample. The experimental

394 Young's modulus of stack bond prisms showed to be in good agreement with the values

395 E_2 of core samples, i.e. when the stress was computed according to the cross-section of

396 the regularized cap. The CV was only 6.6% in this case. Lower values were obtained for

397 E_1 of core samples, i.e. when the stress related to the entire diametric cross-section of the

398 core samples was considered in the calculations.

399 The experimental values of the compressive strength of masonry ranged between 3.98

400 MPa and 6.17 MPa, depending on the type of sample. The maximum strength was

401 provided by f_{C2} of the core samples 2JC. As for the core samples, the presence of the

402 vertical mortar joint resulted in an average reduction of the compressive strength of -

403 6.3%. However, this difference between the strengths of 2JCs and 3JCs actually depends

17

on the condition and integrity of the head joint. It is worth mentioning that the head joints are often badly executed in existing masonry, i.e. they may have been partially filled by the masons during the construction. For this reason, other experimental programs on masonry characterised by partially filled head joints might result in a higher discrepancy between the 2JC and 3JC compressive strengths.

It is worth mentioning that the calculation of the compressive strength f_{C2} obtained from the tests on the cylindrical cores considering the width of the cap is much closer to the compressive strength of the prisms than f_{C1}, calculated considering the diameter of the cylinders. The coefficient of variation was only 3%.
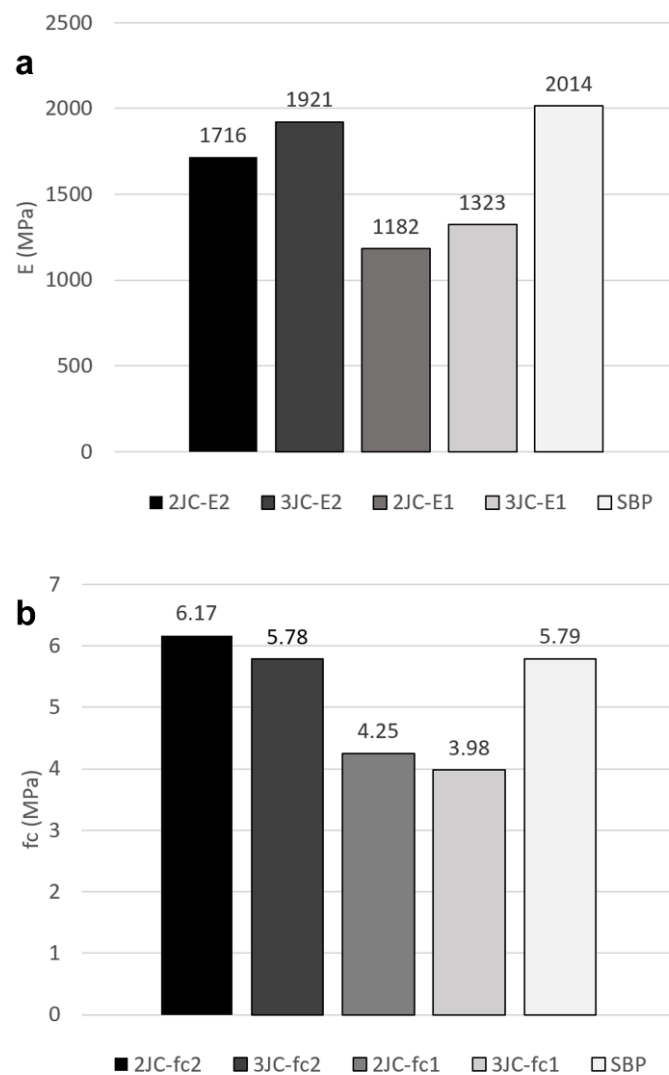
Figure 10 – Comparison between compression tests on cylindrical samples and stack bond prisms: a) Young's modulus, b) compressive strength.

18

418   The ratios between the experimental Young's moduli and compressive strengths obtained
419   for the different specimens were 278 for 2JCs, 332 for 3JCs, and 347 for stack bond
420   prisms. All the obtained values are much lower than the ratios suggested by the current
421   European and American standards, such as 1000 by CEN [31] and 700 by ACI [32]. This
422   disagreement suggests that the reference ratios provided by these standards are not
423   suitable for aerial lime mortar and brick masonry. On the other hand, the Italian standards
424   [33] suggest typical ratios around 450 for masonry made of solid bricks and lime mortar.

4. Numerical simulation of compression tests on cylindrical samples

427   The extraction of cylindrical samples from existing masonry walls shows to be a very
428   useful minor destructive technique for the evaluation of the compressive strength of
429   existing masonry structures. Nevertheless, the presented experimental results illustrate
430   some difficulties in the interpretation of the experimental results, such as the choice of
431   the effective resistant area of the cylindrical samples, which is used for the determination
432   of the compressive strength of aerial lime mortar and brick masonry. This section aims to
433   provide a numerical insight into the evolution of the resisting and failure mechanisms of
434   2JCs and 3JCs.

4.1 Numerical models

436   The cylindrical samples are simulated by using a continuum finite element approach with
437   distinct modelling of the mortar, the brick and the regularization mortar cap [22]. Figure
438   11 illustrates the used finite element meshes for the 2JCs and 3JCs. These are composed
439   of 8208 isoparametric solid brick elements (9800 nodes) based on linear interpolation and
440    $2 \times 2 \times 2$ Gauss integration. Only a quarter of the specimen is modelled, while proper
441   symmetrical boundary conditions restraining only horizontal displacements are imposed
442   to the interior surfaces of the specimen along the two vertical planes of symmetry to
443   consider the effect of the non-modelled parts of the cylinders. The experiment is
444   simulated by applying a vertical incremental displacement at the top of the regularization
445   cap, precluding horizontal displacement, while the lower end is kept fixed. The system of
446   nonlinear equilibrium equations is solved at each analysis step through the use of a secant
447   method along with a line-search procedure. Convergence is attained when the ratio
448   between the norm of the iterative residual forces and the norm of the total external forces

449　is lower than 10^{-2} (1%). The simulations are performed using the finite element analysis

450　software COMET [34], while GiD [35] is used for the pre- and post-processing, both

451　developed at the International Centre for Numerical Methods in Engineering (CIMNE) in

452　Barcelona, Spain.
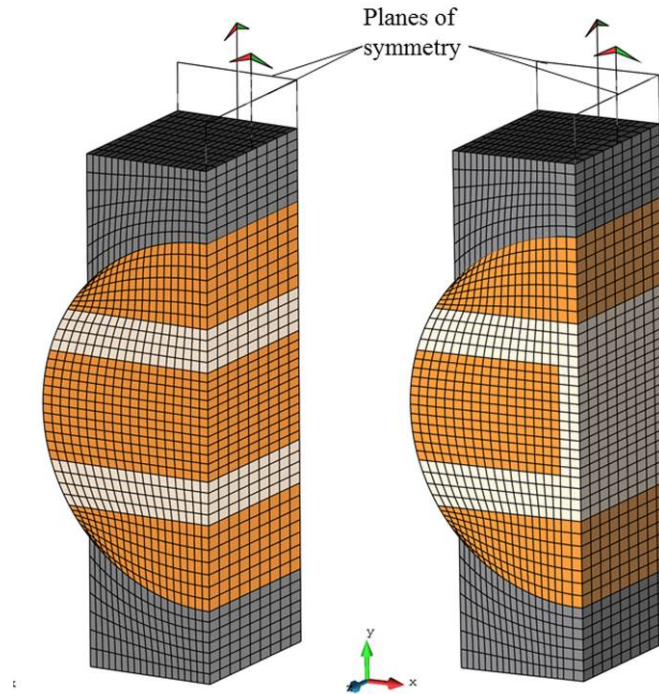
453

454　Figure 11 – Finite element meshes used in the numerical simulations for the two joint cylinder (left) and

455　the three joint cylinder (right). The planes of symmetry are those having a normal vector with direction

456　towards the +x and the –z.

457

458　Table 6 presents the mechanical properties of the brick and mortar used in the numerical

459　model. The tensile strength (f_t) for both materials was defined using the experimental

460　results of the flexural tests and the expressions proposed by CEB-FIB [36]. The

461　normalized uniaxial compressive strength of the bricks was measured through uniaxial

462　compressive tests, presented in Table 2, and by applying the shape factor equal to 0.7

463　recommended by CEN [26]. The uniaxial compressive strength of the mortar was

464　estimated through the DPT on mortar joints extracted from the dismantled wall of Figure

465　2a and presented in Table 3. The Young's modulus of the units was measured in [15] by

466　adopting the experimental procedure proposed for concrete by CEN [37]. The adopted

467　value is the average given from cylinders extruded from the lateral sides of the brick

468　(header and stretcher) and for cyclic loading up to 60% of unit's maximum force [15].

469　The Young's modulus of the mortar was defined such that the elastic stiffness of the

470   numerical model was equivalent to that of the experimental one of the specimens 2JC4,

471   2JC13 and 2JC15 at the beginning of the experiment, which presented the highest

472   stiffness. The formula suggested by the standard [36] has been used for the tensile fracture

473   energy (G_{ft}), while the compressive fracture energy (G_{fc}) was the result of a sensitivity

474   analysis aimed at obtaining a good agreement with the experimental results in the post

475   peak nonlinear range. Linear elastic behaviour is assumed for the regularization cap with

476   a Young's modulus equal to 23000 MPa.

477   Table 6 – Mechanical properties of brick and mortar used in the numerical simulations

Property	Brick	Mortar
E (MPa)	7140	100
ν (−)	0.18	0.25
f_t (MPa)	1.64	0.24
f_c (MPa)	21.49	0.91
G_{ft} (J/m^2)	126	80
G_{fc} (J/m^2)	34400	1440
f_{c0} (MPa)	10.75	0.405
ε_{pc} (−)	0.025	0.045
f_{bc}/f_c	1.15	1.5
ρ (−)	0.75	0.75

478

479   The numerical analysis simulates the cracking and crushing of the mortar and bricks by

480   using a continuum damage mechanics model with damage induced orthotropic behaviour

481   along the principal axes [38]. The model uses two distinct damage indices to distinguish

482   between tensile and compressive damage. The tensile response is characterised by a linear

483   part until reaching the peak strength, and the post-peak part with an exponential softening

484   law. For the compressive damage, the constitutive law presented in [39] is adopted,

485   allowing for a parabolic hardening-softening part followed by exponential softening.

486   Table 6 presents the selected values of the elastic limit of the compressive strength (f_{c0})

487   and the strain (ε_{pc}) for the peak compressive strength (f_c) for each material. For both tensile

488   and compressive laws, a residual strength equals to 10% of the maximum capacity is used.

489   The adopted failure criterion is the one presented by Lubliner et al. [40]. The ratio

490   between biaxial and uniaxial compressive strength (f_{bc}/f_c) is defined equal to 1.15 for the

491   units and 1.50 for the mortar. Parameter ρ defines the shape of the compressive failure

492   surface under triaxial compression and is considered equal to 0.75 for both units and

493   mortar. The latter values for f_{bc}/f_c and ρ are selected based on a sensitivity analysis due to

494   the difficulty of their derivation from standard experimental procedures.

4.2 Numerical simulation of compression tests on two joint cylinders

Figure 12 presents the graphs of experimental and numerical force against vertical displacement at the top of the cap for the case of the 2JCs. For each experimental graph, the loading-unloading cycles are omitted and the part of the graph before them (not included in Figure 6b,d) is reproduced using the tangent to the curve after the end of the cycles.
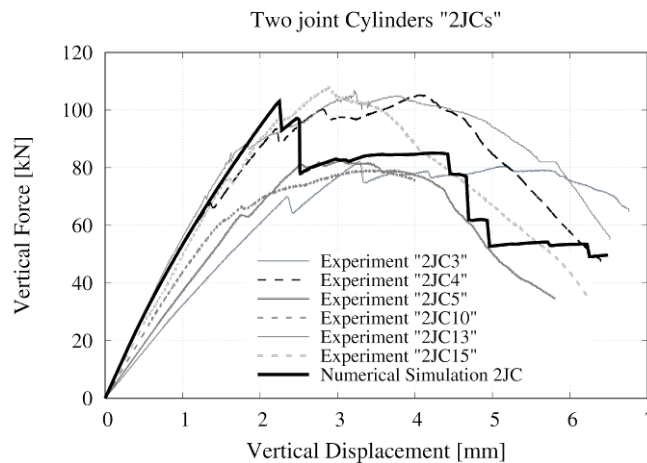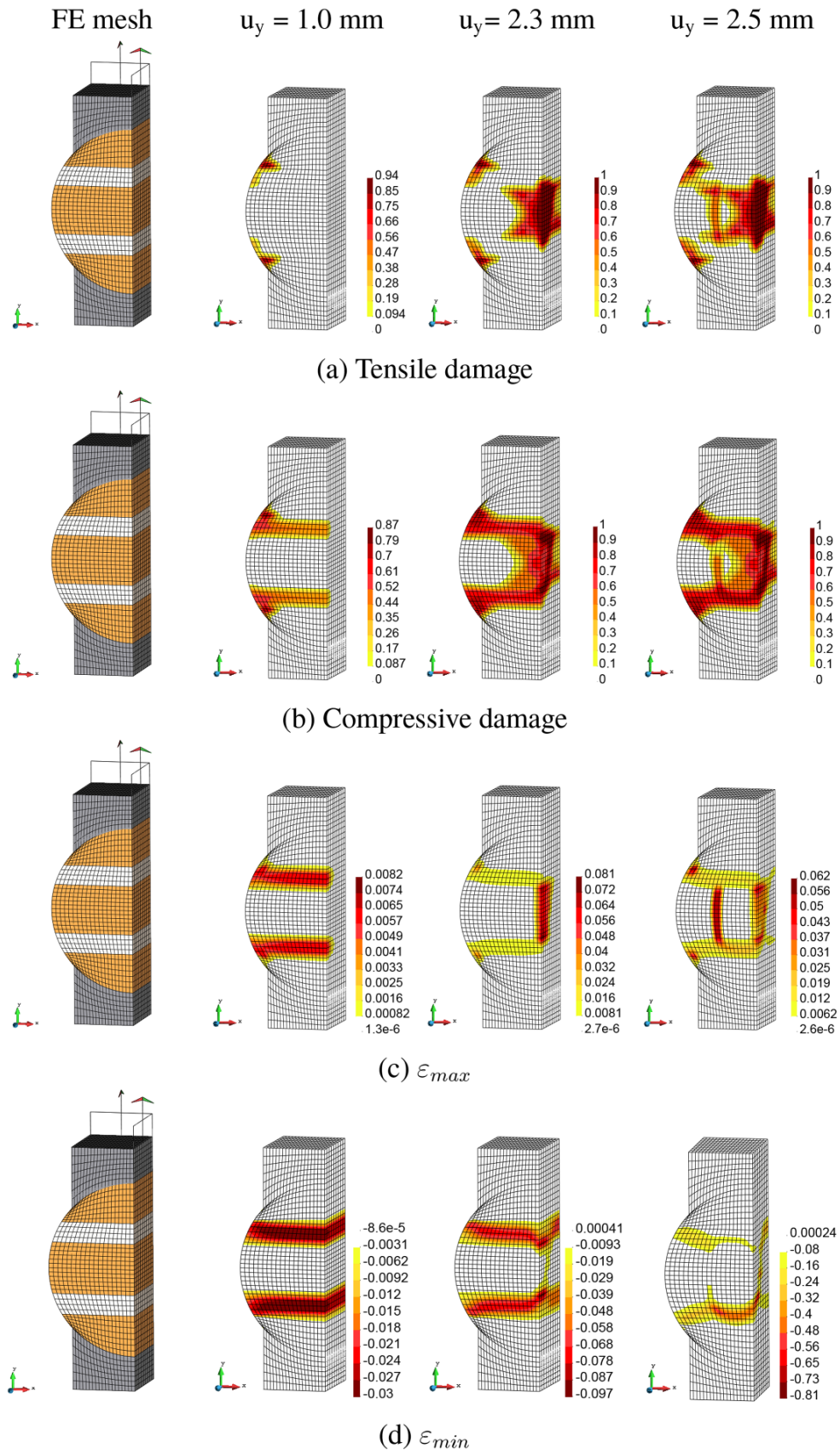

Figure 12 – Two joint cylinder specimens: graphs of experimental and numerical force against displacement at the top of the sample.

As said in the previous Section 5.1, the calibration of the Young's modulus of the mortar has been based on specimens 2JC4, 2JC13 and 2JC15, which present the highest stiffness. For this reason, the stiffness and capacity predicted by the numerical simulation are very close to those given by the particular cylindrical specimens. It is noted that after the value of the mortar's Young's modulus was calibrated for the 2JCs, the same value was also used for the 3JCs, presented in the following Section 5.3. The numerical simulation predicts a peak strength of 103.0 kN. This value falls within the limits given by the experimental results, which are between 79.1 kN for 2JC13 and 107.9 kN for 2JC15. The simulation shows that the first cracks in the cylinder appear close to the lateral edge of the regularization cap and affect mostly the upper and lower bricks and less the mortar joints. At this stage of the analysis, presented in the second column of Figure 13 (for a vertical displacement $u_y = 1.0$ mm), most compressive damage exists at the external parts of the mortar joints. The lower capacity of the external part of the mortar joints compared to the internal part is due to its different stress state. As shown in Figure 14, the external parts of the mortar joints are under a tension-compression stress state, while the internal parts are under triaxial compression allowing them to sustain higher compression. The

22

first drop of the capacity occurs for a vertical displacement at the top $u_y = 2.3$ mm and is associated to the opening of a crack at the middle of the central brick (third column of Figure 13). The compressive damage at the brick (Figure 13b) occurs under a tension-compression stress state. Compressive damage evolves also at the external parts of the mortar joints. After the appearance of the central crack, the cylinder recovers some of the capacity up to a vertical displacement $u_y = 2.5$ mm, when a second crack appears at the central brick (fourth column of Figure 13). The new crack results in the partial closure of the central one, as demonstrated from the contour of the maximum principal strains in Figure 13c. The rest of the analysis leads to the increase of the degradation of the mortar and the brick at the already damaged locations. When the tensile or compressive fracture energy is exhausted at one of these parts, another drop is obtained in the capacity curve (Figure 12).

FE mesh $u_y = 1.0$ mm $u_y = 2.3$ mm $u_y = 2.5$ mm

(a) Tensile damage

(b) Compressive damage
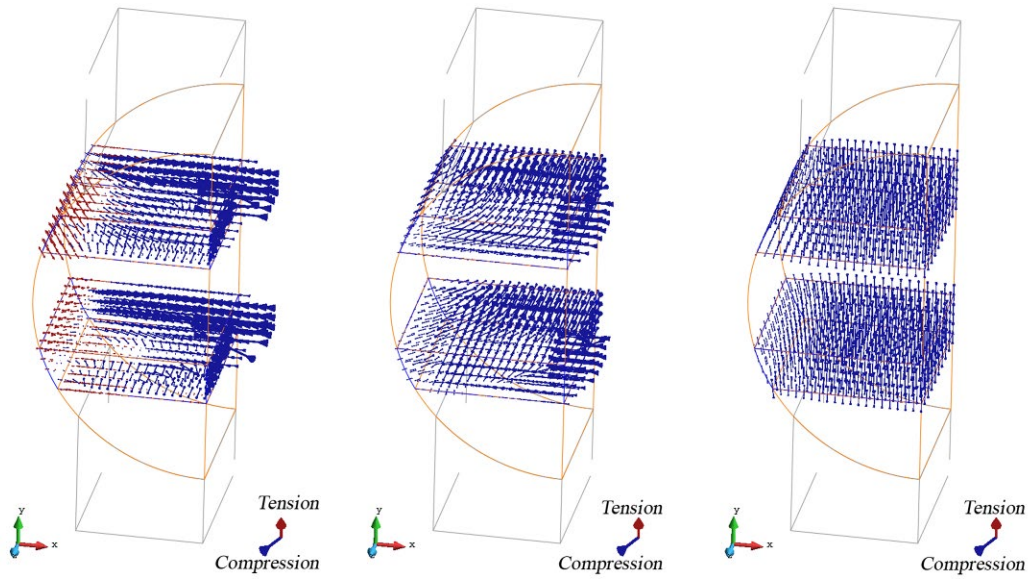

(c) ε_{max}

(d) ε_{min}

534

535   Figure 13 – Numerical simulation of two joint cylinder specimens: evolution of (a) tensile damage, (b)

536   compressive damage, (c) maximum principal strains ε_{max} and (d) minimum principal strains ε_{min} for

537   different levels of vertical displacement.

538

539

540   Figure 14 – Numerical simulation of two joint cylinder specimens: vectors of the principal stresses at the

541   mortar joints for a vertical displacement of $u_y = 1$ mm: (a) σ_I (b) σ_{II} and (c) σ_{III}.
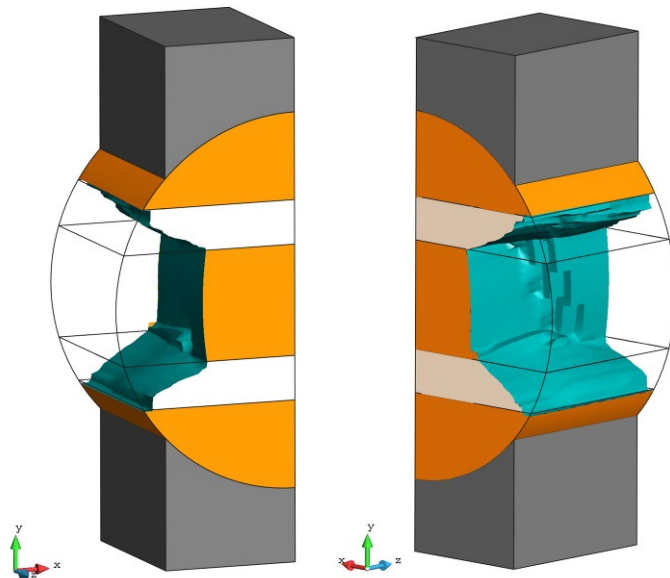
542

543   Figure 15 presents the crack surface in the two joint cylinder at the end of the numerical

544   simulation, as the isosurface of horizontal displacements of 1 mm. The numerical

545   simulation predicts correctly the typical hourglass failure observed in the experimental

546   results (Figure 7a).


547

548   Figure 15 – Numerical simulation of two joint cylinder specimens: final failure pattern shown as the

549   isosurface of horizontal displacements u_x of 1 mm

550

551   The presented numerical analysis of the 2JCs has provided an insight into their resistant
552   part during the compression tests, useful to understand how to evaluate their compressive
553   strength. Figure 16 presents the distribution of the vertical stresses (σ_{yy}) at the middle of
554   the mortar joint and the central brick for the 2JC in two instances of the numerical
555   analysis. Before damage occurs to the central brick (Figure 16a), a similar stress profile
556   is observed within both the mortar and the brick, with the vertical stresses increasing from
557   the exterior to the interior and center of the cylinder. After the opening of the central
558   crack, a stress redistribution occurs within the brick, affecting mostly the front part close
559   to front face of the cylinder. This is because the central crack does not propagate through
560   the whole length of the cylinder, as also observed in the fourth column of Figure 13.
561   Regarding the mortar, the increase of the compressive damage at the external faces,
562   reduces significantly the level of the vertical stresses at these locations. The interior part
563   though, presents a plateau of high vertical stresses. Overall, the vertical stress distribution
564   during the different stages of the simulation shows that the size of the regularization cap
565   delimits the actual resisting area of the 2JC.
566
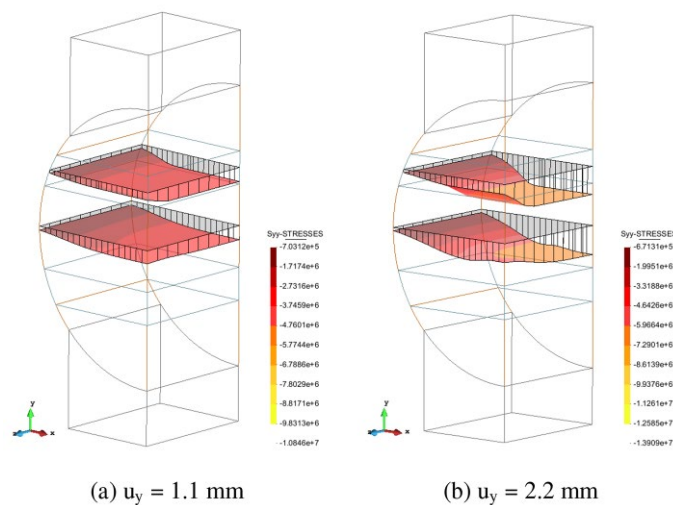
(a) $u_y = 1.1$ mm   (b) $u_y = 2.2$ mm

Figure 16 – Numerical simulation of two joint cylinder specimens: vertical stress distribution σ_{yy} (a) before the opening of the central crack and (b) before the opening of the external crack at the central brick.

4.3 Numerical simulation of compression tests on three joint cylinders

572   Figure 17 presents the graphs of experimental and numerical force against vertical
573   displacement at the top of the cylinder for the case of the 3JCs. As for the 2JCs, the part
574   before the loading-unloading cycles is reproduced using the tangent to the curve after the
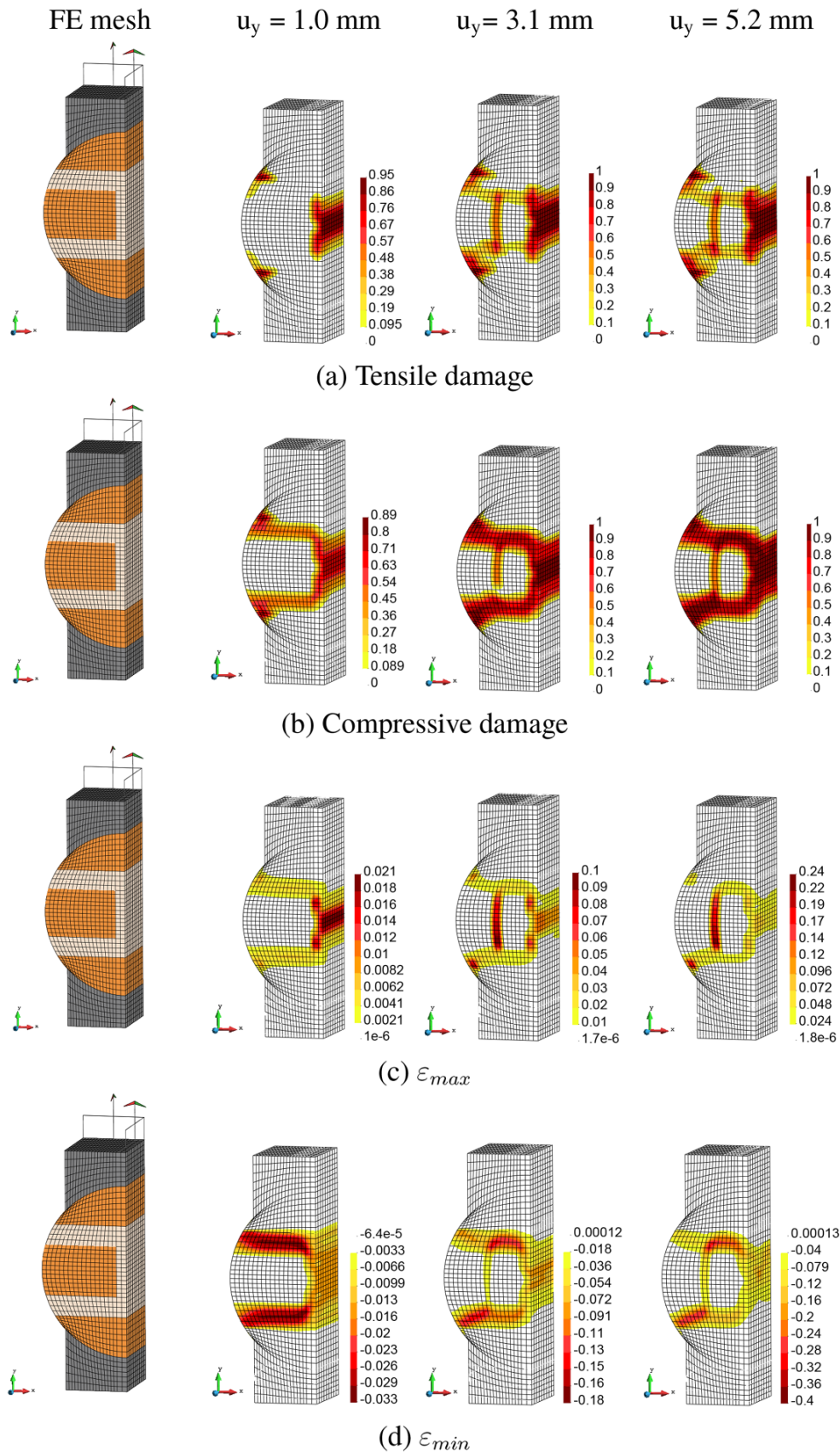
26

575   end of the cycles. The numerical analysis predicts a capacity of 96.7 kN for the 3JCs,

576   which falls within the limits of the experimental results defined by the capacity of 3JC2

577   and 3JC8 samples of 74.6 kN and 104.9 kN, respectively. Similar to the experimental

578   results, the numerical simulations predict a reduction of the capacity of the cylindrical

579   cores due to the presence of the vertical joint of -5.9%. This value is very close to the

580   experimentally measured reduction in the capacity of the cylinders of -6.3%, see Table 4

581   and Figure 10. The numerical simulation represents the ideal case of a perfectly filled

582   head joint attached to the central brick, which is rarely the case of existing masonry. This

583   fact justifies the slightly lower reduction of the capacity due to the existence of the head

584   joint compared to the experimental results.
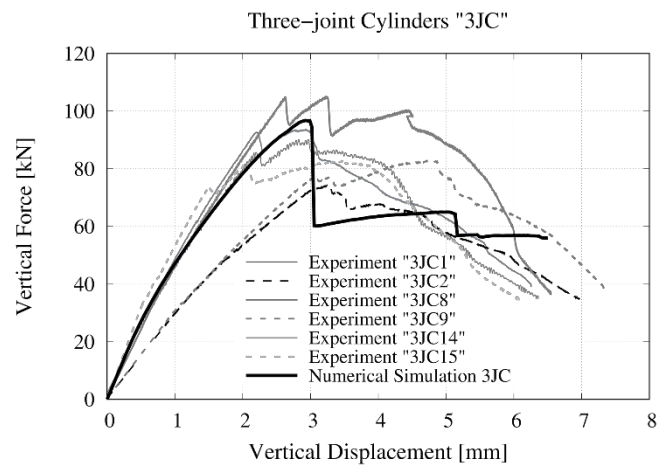
585

586   Figure 17 – Three joint cylinder specimens: graphs of experimental and numerical force against

587   displacement at the top of the sample.

588

589   The first damage in the 3JC are the cracks at the top and bottom bricks close to their

590   connection with the regularization mortar cap (second column of Figure 18a). Compared

591   to the 2JC, the low tensile strength of the mortar leads to the appearance of the vertical

592   crack at the central head joint for low levels of loading. This crack results in the gradual

593   loss of the stiffness of the specimen until reaching the peak load for a vertical

594   displacement at the top of the cylinder $u_y = 3.1$ mm. The drop of the capacity coincides

595   with the appearance of another crack in the central brick, see third row of Figure 18. From

596   that point on, compressive and tensile damage continues to increase in the already

597   damaged locations, as can be seen in the last column of Figure 18. The second drop of

598   the capacity, shown in Figure 17, coincides with the compressive failure of a part of the

599   lower mortar joint.

600

27

FE mesh   u_y = 1.0 mm   u_y= 3.1 mm   u_y = 5.2 mm

(a) Tensile damage

(b) Compressive damage

(c) ε_{max}

(d) ε_{min}

601

602 Figure 18 – Numerical simulation of three joint cylinder specimens: evolution of (a) tensile damage, (b)

603 compressive damage, (c) maximum principal strains ε_{max} and (d) minimum principal strains ε_{min} for

604 different levels of vertical displacement.

605

606 The numerical simulation predicts also for the 3JC the typical hourglass failure as in the

607 experimental results (Figure 7b). The surface of the lateral crack in the central brick at

608 the end of the analysis and its propagation through the mortar joint is illustrated in Figure

609 19.
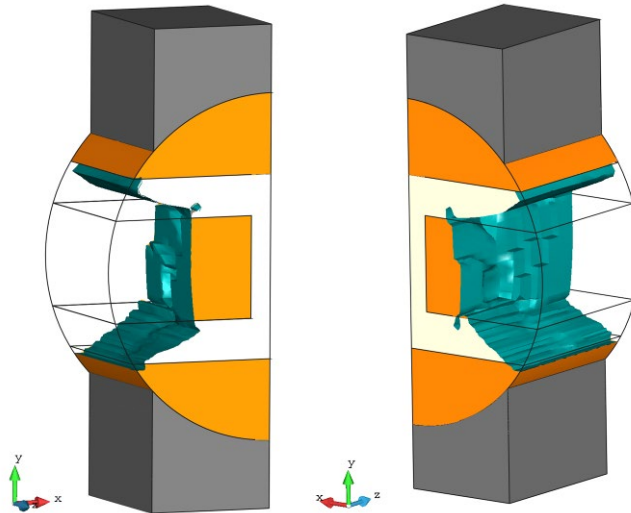
610

611 Figure 19 – Numerical simulation of three joint cylinder specimens: final failure pattern shown as the

612 isosurface of horizontal displacements u_x of 5 mm

613

614 Similar to the 2JC, Figure 20 presents the vertical stress distribution σ_{yy} at the middle of

615 the top bed joint and at the middle of the central brick and the head joint at two stages of

616 the numerical simulation. The stress distribution is similar to that of the 2JC, with the

617 exception of the lower stress gradients at the location of the head joint due to the early

618 appearance of the central crack. During the whole length of the simulation, the parts of

619 the cylinder outside the area defined by the regularization cap appear to have a limited

620 contribution to the sustainment of the imposed vertical load.

621
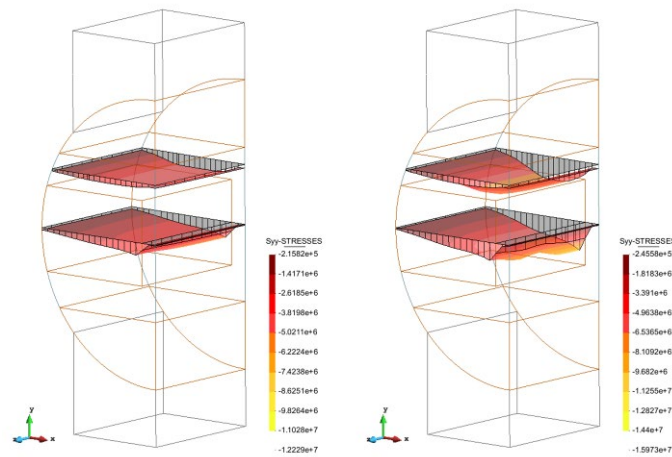
(a) u_y = 1.3 mm   (b) u_y = 2.6 mm

Figure 20 – Numerical simulation of three joint cylinder specimens: vertical stress distribution σ_{yy} (a) at an early stage of the analysis with the crack at the head joint already opened and (b) before the opening of the external crack at the central brick.

5. Conclusions

This research has presented an experimental and numerical investigation of the laboratory compression test of cylindrical samples core drilled from masonry walls. A specific type of traditional masonry has been considered, composed of handmade terracotta solid bricks and aerial lime mortar joints. Such material is frequent in existing construction, especially in the structures of the built heritage.

Two walls were built in the laboratory with the aim of reproducing the in-situ sampling and subsequent testing of masonry cores. One year after the construction, 150 mm diameter cylindrical specimens were extracted from the walls by using a dry core-drilling procedure (without water) in order to avoid disjointing of the samples. Some of the cores (2JC) presented two horizontal mortar joints, whereas some others had two horizontal mortar joints plus a vertical one (3JC). The cylindrical samples were regularized by using high strength mortar caps and then tested in the laboratory under compression. Stack bond prisms were also built and tested at the same time, in order to have a direct comparison between the novel tests on extracted cylindrical samples and the tests on prismatic samples conforming to the current standards for new construction.

The materials used in the present experimental campaign have presented low-to-moderate mechanical properties, with a normalized compressive strength of bricks of 21.5 MPa and a compressive strength of mortar of 1.63 MPa after 1 year of curing. The experimental tests on masonry samples have shown that a compressive strength above 4 MPa can be

30

646   obtained by using aerial lime mortar with proper carbonation level (mature period) and

647   moderately strong units.

648   The average compressive strength of stack bond prisms has been 5.79 MPa, i.e. 3.6 times

649   higher than the compressive strength of the mortar after one year of curing. The average

650   Young's modulus of stack bond prisms, of 2014 MPa, has provided a ratio to the

651   compressive strength equal to 347.

652   As for the cylindrical samples, besides the 3JCs suggested by the UIC 778-3R guidelines

653   [18], this research program has considered a type of cylindrical sample, identified as 2JCs,

654   which does not include the vertical joint, in order to assess its effect on the measured

655   strength. The 2JCs have provided an average compressive strength 6.3% higher than the

656   3JCs. However, this value may vary depending on the condition of integrity of head joints

657   in the existing brickwork.

658   The compression test on 150 mm diameter cylinders has shown to be an appropriate

659   technique for the evaluation of the compressive capacity of existing masonry. The

660   hourglass type of failure has been observed in both 2JCs and 3JCs. The compressive

661   strengths from core samples have resulted in a good agreement with those derived from

662   the standard tests on stack bond prisms. However, the compressive strength of cylindrical

663   specimens has to be calculated carefully. This work has evaluated it by making use of two

664   extreme values, based on the assumptions of either a total diametric or a cap wide resisting

665   cross-section [14,15]. The present study has shown that the second estimate (6.17 MPa

666   for 2JCs and 5.78 MPa for 3JCs) provides compressive strength values more in agreement

667   with those from stack bond prisms. The values of the Young's modulus of the core

668   samples have shown a good agreement with the results from the standard tests when, once

669   again, the cap wide resisting cross-section is considered in calculation.

670   The paper has presented also the numerical simulation of the compression tests of the

671   2JCs and 3JCs with the aim to interpret their resisting mechanism and identify the

672   procedure for the calculation of the compressive strength. The finite element micro-

673   modelling technique has been considered for this purpose. The numerical simulations

674   have predicted correctly the capacity given by the experimental results and the hourglass

675   failure mechanism of both the 2JCs and 3JCs. The vertical stress distributions within the

676   FEM models of the cylinders indicate that the parts outside the regularization parts have

677   a limited contribution to the resistance of the specimen under compressive loading. The

678   numerical study has complemented the experimental outcomes with further insight into

679 the mechanical behaviour of the extracted cylindrical specimens when tested under
680 compression.

681 The research has presented an experimental and numerical understanding of a technique
682 intended to assist experts working in the analysis of historical buildings, who are
683 constantly in need for reference values for specific typologies of masonry and also require
684 reliable validation criteria for the non-standard tests on samples extracted from existing
685 structural members. Following this line, it is highly advisable to continue investigating
686 and improving the experimental MDT procedures based on core drilling and testing of
687 cylindrical samples, as they have shown to be very promising and minimally invasive. At
688 the same time, the enlargement of the database of experimental results for other
689 typologies of masonry materials is also suggested, in order to obtain more data allowing
690 to validate and extend the prescriptions of the current technical standards applicable to
691 existing masonry structures.

692

706

References

708 [1]   A.W. Page, The Biaxial Compressive Strength of Brick Masonry, Proc. Inst. Civ. Eng. 71 (1981)
709   893–906. doi:10.1680/iicep.1981.1825.
710 [2]   G. Baronio, L. Binda, A. Saisi, Analisi di Malte Antiche e Comportamento di Malte Riprodotte in

711		Laboratorio (in Italian), in: 7° Convegno Naz. - L'ingegneria Sismica Ital., Collegio degli
712		Ingegneri della Toscana, Siena, Italy, 1995: pp. 267–276.
713	[3]	G. Baronio, L. Binda, A. Saisi, Mechanical and Physical Behaviour of Lime Mortars Reproduced
714		After the Characterisation of Historic Mortar, in: P. Bartos, C. Groot, J.J. Hughes (Eds.), Int.
715		RILEM Work. Hist. Mortars Charact. Tests, 1999: pp. 307–325.
716	[4]	Y. Boffill, H. Blanco, I. Lombillo, L. Villegas, Assessment of historic brickwork under
717		compression and comparison with available equations, Constr. Build. Mater. 207 (2019) 258–
718		272. doi:10.1016/j.conbuildmat.2019.02.083.
719	[5]	CEN, EN 1052-1:1998 Methods of test for masonry - Part 1: Determination of compressive
720		strength, (1998).
721	[6]	RILEM, Technical recommendations for testing and use of constructions materials: LUM B1 –
722		Compressive strength of small walls and prisms, (1991) 474–477. doi:10.1617/2351580117.147.
723	[7]	A. Drougkas, P. Roca, C. Molins, Compressive strength and elasticity of pure lime mortar
724		masonry, Mater. Struct. 49 (2016) 983–999. doi:10.1617/s11527-015-0553-2.
725	[8]	J. Segura, L. Pelà, P. Roca, Monotonic and cyclic testing of clay brick and lime mortar masonry
726		in compression, Constr. Build. Mater. 193 (2018) 453–466.
727		doi:10.1016/j.conbuildmat.2018.10.198.
728	[9]	A. Aprile, A. Benedetti, F. Grassucci, Assessment of Cracking and Collapse for Old Brick
729		Masonry Columns, J. Struct. Eng. 127 (2001) 1427–1435. doi:10.1061/(ASCE)0733-
730		9445(2001)127:12(1427).
731	[10]	N. Domède, G. Pons, A. Sellier, Y. Fritih, Mechanical behaviour of ancient masonry, Mater.
732		Struct. 42 (2009) 123–133. doi:10.1617/s11527-008-9372-z.
733	[11]	L. Binda, G. Fontana, G. Frigerio, Mechanical behaviour of brick masonries derived from units
734		and mortar characteristics, in: 8th Int. Brick Block Mason. Conf., Dublin, 1988: pp. 205–216.
735	[12]	L. Binda, C. Tiraboschi, S. Abbaneo, Experimental research to characterise masonry materials,
736		Mason. Int. 10 (1997) 92–101.
737	[13]	L. Binda, G. Mirabella Roberti, C. Tiraboschi, Problemi di misura dei parametri meccanici della
738		muratura e dei suoi componenti (in Italian), in: La Mecc. Delle Murature Tra Teor. e Progett.,
739		Messina, Italy, 1996: pp. 45–54.
740	[14]	L. Pelà, P. Roca, A. Benedetti, Mechanical Characterization of Historical Masonry by Core
741		Drilling and Testing of Cylindrical Samples, Int. J. Archit. Herit. 10 (2016) 360–374.
742		doi:10.1080/15583058.2015.1077906.
743	[15]	L. Pelà, E. Canella, A. Aprile, P. Roca, Compression test of masonry core samples extracted from
744		existing brickwork, Constr. Build. Mater. 119 (2016) 230–240.
745		doi:10.1016/j.conbuildmat.2016.05.057.
746	[16]	D. Marastoni, L. Pelà, A. Benedetti, P. Roca, Combining Brazilian Tests on masonry cores and
747		Double Punch Tests for the mechanical characterization of historical mortars, Constr. Build.
748		Mater. 112 (2016) 112–127. doi:10.1016/j.conbuildmat.2016.02.168.
749	[17]	L. Pelà, K. Kasioumi, P. Roca, Experimental evaluation of the shear strength of aerial lime mortar
750		brickwork by standard tests on triplets and non-standard tests on core samples, Eng. Struct. 136

751   (2017) 441–453. doi:10.1016/j.engstruct.2017.01.028.

752   [18]   International Union of Railways, Leaflet 778-3R, Recommendations for the inspection,

753   assessment and maintenance of masonry arch bridges, (2011).

754   [19]   A. Brencich, C. Corradi, E. Sterpi, Experimental Approaches to the Compressive Response of

755   Solid Clay Brick Masonry, in: 13th Int. Brick Block Conf., Amsterdam, NL, 2004: pp. 1–10.

756   [20]   A. Brencich, E. Sterpi, Compressive Strength of Solid Clay Brick Masonry : Calibration of

757   Experimental Tests and Theoretical Issues, in: P.B. Lourenço, P. Roca, C. Modena, S. Agrawal

758   (Eds.), Struct. Anal. Hist. Constr., New Delhi, India, 2006: pp. 757–766.

759   [21]   C. Bilello, A. Brencich, C. Corradi, M. Di Paola, E. Sterpi, Experimental Tests and Theoretical

760   Issues for the Identification of Existing Brickwork, in: 10th North Am. Mason. Conf., St. Louis,

761   Missouri, USA, 2007: pp. 964–974.

762   [22]   M. Petracca, L. Pelà, R. Rossi, S. Zaghi, G. Camata, E. Spacone, Micro-scale continuous and

763   discrete numerical models for nonlinear analysis of masonry shear walls, Constr. Build. Mater.

764   149 (2017) 296–314. doi:10.1016/j.conbuildmat.2017.05.130.

765   [23]   A. Drougkas, P. Roca, C. Molins, Numerical prediction of the behavior, strength and elasticity of

766   masonry in compression, Eng. Struct. 90 (2015) 15–28. doi:10.1016/j.engstruct.2015.02.011.

767   [24]   CEN, EN 459-1:2010 Building lime - Part 1: Definitions, specifications and conformity criteria,

768   (2010).

769   [25]   CEN, EN 1015-11:2007 Methods of test for mortar for masonry - Part 11: Determination of

770   flexural and compressive strength of hardened mortar, (2007).

771   [26]   CEN EN772-1, Methods of Test for Masonry Units. Part 1: Determination of the Compressive

772   Strength, Comité Européen de Normalisation, Brussels, 2000.

773   [27]   A.W. Page, R. Marshall, The influence of brick and brickwork prism aspect ratio on the

774   evaluation of compressive strength, in: T. McNeilly, J.C. Scrivener (Eds.), 7th Int. Brick Block

775   Mason. Conf. (IB2MAC 1985), Melbourne, 1985: pp. 653–664.

776   [28]   DIN 18555-9:1999, Testing of mortars containing mineral binders - Part 9: Hardened mortars.

777   Determination of the mortar compressive strength in the bed joint, 1999.

778   [29]   J. Henzel, S. Karl, Determination of Strength of Mortar in the Joints of Masonry by Compression

779   Tests on Small Specimens, Darmstadt Concr. 2 (1987) 123–136.

780   [30]   K. Kasioumi, Experimental Testing on Cylindrical Specimens of Aerial Lime Mortar Masonry,

781   SAHC Master dissertation. Technical University of Catalonia, 2015.

782   [31]   EN 1996-1-1:2005, Eurocode 6: Design of masonry structures – Part 1-1: General rules for

783   buildings – rules for reinforced and unreinforced masonry, (2005).

784   [32]   ACI, ACI 530-05, Building Code Requirements for Masonry Structures, 2011.

785   [33]   Circolare 21 gennaio 2019, n. 7 C.S.LL.PP. Istruzioni per l'applicazione dell'«Aggiornamento

786   delle "Norme tecniche per le costruzioni"» di cui al decreto ministeriale 17 gennaio 2018 (in

787   Italian), (2019).

788   [34]   COMET, Coupled Mechanical and Thermal analysis, http://www.cimne.com/comet/, (2016).

789   [35]   GiD v.14, The personal pre and post-processor, http://www.gidhome.com/, (2018).

790   [36]   fib, fib Model Code for Concrete Structures 2010, Wiley-VCH Verlag GmbH & Co. KGaA,

791   Weinheim, Germany, 2013. doi:10.1002/9783433604090.

792 [37] CEN EN12390-13, Testing hardened concrete. Determination of secant modulus of elasticity in

793   compression, Comité Européen de Normalisation, Brussels, 2013.

794 [38] R. Faria, J. Oliver, M. Cervera, A strain-based plastic viscous-damage model for massive

795   concrete structures, Int. J. Solids Struct. 35 (1998) 1533–1558. doi:10.1016/S0020-

796   7683(97)00119-4.

797 [39] M. Petracca, L. Pelà, R. Rossi, S. Oller, G. Camata, E. Spacone, Regularization of first order

798   computational homogenization for multiscale analysis of masonry structures, Comput. Mech. 57

799   (2016) 257–276. doi:10.1007/s00466-015-1230-6.

800 [40] J. Lubliner, J. Oliver, S. Oller, E. Oñate, A plastic-damage model for concrete, Int. J. Solids

801   Struct. 25 (1989) 299–326. doi:10.1016/0020-7683(89)90050-4.

802

Highlights

804 • Construction and one year curing of aerial lime mortar and brick masonry walls

805 • Extraction of core samples from masonry walls to simulate MDT in-situ sampling

806 • Comparison between compressive parameters from core samples and stack bond

807 prisms

808 • Numerical simulation by FEM micromodelling of compression testing of core samples

809 • Calculation of compressive parameters from cores considering cap's cross-section

810